Research
Environmental Engineering—Article

Efficient H$_2$O$_2$ Electrosynthesis and Its Electro-Fenton Application for Refractory Organics Degradation

Lei Li [a], Jing Bai [a,b,*], Panyu Jiang [a], Yan Zhang [a], Tingsheng Zhou [a], Jiachen Wang [a], Changhui Zhou [a], Jinhua Li [a], Baoxue Zhou [a,b,*]

[a] School of Environmental Science and Engineering, Key Laboratory of Thin Film and Microfabrication Technology (Ministry of Education), Shanghai Jiao Tong University, Shanghai 200240, China
[b] Shanghai Institute of Pollution Control and Ecological Security, Shanghai 200092, China

ARTICLE INFO

ABSTRACT

Hydrogen peroxide (H$_2$O$_2$) *in situ* electrosynthesis by O$_2$ reduction reaction is a promising alternative to the conventional Fenton treatment of refractory wastewater. However, O$_2$ mass transfer limitation, cathodic catalyst selectivity, and electron transfer in O$_2$ reduction remain major engineering obstacles. Here, we have proposed a systematic solution for efficient H$_2$O$_2$ generation and its electro-Fenton (EF) application for refractory organic degradation based on the fabrication of a novel ZrO$_2$/CMK-3/PTFE cathode, in which polytetrafluoroethylene (PTFE) acted as a hydrophobic modifier to strengthen the O$_2$ mass transfer, ZrO$_2$ was adopted as a hydrophilic modifier to enhance the electron transfer of O$_2$ reduction, and mesoporous carbon (CMK-3) was utilized as a catalyst substrate to provide catalytic active sites. Moreover, feasible mass transfer of O$_2$ from the hydrophobic to the hydrophilic layer was designed to increase the contact between O$_2$ and the reaction interface. The H$_2$O$_2$ yield of the ZrO$_2$/CMK-3/PTFE cathode was significantly improved by approximately 7.56 times compared to that of the conventional gas diffusion cathode under the same conditions. The H$_2$O$_2$ generation rate and Faraday efficiency reached 125.98 mg·cm^{-2}·h^{-1} (normalized to 5674.04 mmol·g^{-1}·h^{-1} by catalyst loading) and 78.24% at −1.3 V versus standard hydrogen electrode (current density of −252 mA·cm^{-2}), respectively. The high H$_2$O$_2$ yield ensured that sufficient ·OH was produced for excellent EF performance, resulting in a degradation efficiency of over 96% for refractory organics. This study offers a novel engineering solution for the efficient treatment of refractory wastewater using EF technology based on *in situ* high-yield H$_2$O$_2$ electrosynthesis.
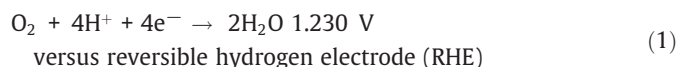
1. Introduction

The widespread application of organic chemicals in various fields increases the possibility of their release into the aquatic environment, which can potentially threaten the natural ecosystem and result in human exposure [1–3]. To address these issues, advanced oxidation processes (AOPs) have received extensive attention in the field of water treatment [4,5]. As typical advanced oxidation technologies, Fenton or Fenton-like processes are widely used owing to their convenience and high pollutant treatment efficiency [6]. However, because the industrial production of H$_2$O$_2$

involves large energy consumption and organic waste output [7], the Fenton process usually suffers from high H$_2$O$_2$ costs [8]. Consequently, it is particularly important to seek a low-cost strategy for efficient on-site H$_2$O$_2$ synthesis for advanced oxidation water-treatment processes [9,10].

The electro-Fenton (EF) reaction, a method with advantage of *in situ* H$_2$O$_2$ generation, which can accelerate the formation of ·OH to degrade organic pollutants, is considered an advanced technique for the treatment of refractory organic pollutants [11,12]. For an efficient EF, a high yield of H$_2$O$_2$ is a prerequisite. To realize a high H$_2$O$_2$ yield, O$_2$ mass transfer, cathodic catalyst selectivity, and electron transfer of O$_2$ reduction need to be enhanced [13–16]. Notably, because oxygen molecules can also be electrically reduced to H$_2$O via the direct 4e$^-$ pathway (Eq. (1)) [17,18], a highly selective cathode catalyst that reduces O$_2$ to H$_2$O$_2$ via the 2e$^-$ route (Eq. (2)) is required.

* Corresponding authors.
E-mail addresses: bai_jing@sjtu.edu.cn (J. Bai), zhoubaoxue@sjtu.edu.cn (B. Zhou).

$$O_2 + 4H^+ + 4e^- \rightarrow 2H_2O \quad 1.230 \text{ V}$$
versus reversible hydrogen electrode (RHE) $\qquad$ (1)

$$O_2 + 2H^+ + 2e^- \rightarrow H_2O_2 \quad 0.695 \text{ V versus RHE} \qquad (2)$$

To seek cathodic catalysts with high H_2O_2 selectivity, researchers have made considerable efforts in recent years and found that carbonaceous materials are the best option because of their high catalytic efficiency and stable electrochemical performance [19–24]. Moreover, the abundant free-flowing π electrons in the sp^2 hybrid orbital add to the research interest in carbonaceous materials, particularly for their use in the electrocatalytic oxygen reduction reaction (ORR), which requires electron participation [25,26]. Among the various carbonaceous materials, mesoporous carbon exhibits better H_2O_2 production performance owing to the abundant defect active sites, feasible O_2 mass transfer channel, positive zeta potential, and large BET surface area [27].

For superior O_2 mass transfer, the easier the diffusion and adsorption of O_2 on the carbon material, the faster the catalytic reduction reaction rate, and the higher the H_2O_2 generation efficiency. Because oxygen diffusion in the ORR is a hydrophobic process, the hydrophobic modification of the carbon material may improve O_2 mass transfer and enhance H_2O_2 production. Recent studies have shown that owing to the excellent hydrophobicity of polytetrafluoroethylene (PTFE), its addition to the surface of carbon materials can significantly enhance diffusion and adsorption enrichment of O_2 [28]. Moreover, to tackle the relatively large thickness of common gas diffusion electrodes (GDEs) and the corresponding vulnerability to water flooding [21,29,30], some successful PTFE modifications of GDE have been explored [31,32]. Sheng et al. [33] proposed the use of PTFE to modify the cathode and improve its surface hydrophobicity and found that the modified cathode exhibited significantly enhanced O_2 diffusion and H_2O_2 production. Zhang et al. [28] modified GDE with PTFE to form a superhydrophobic three-phase interface and comparing that with traditional GDE, observed significantly improved O_2 diffusion and adsorption and a 5.7-fold increase in H_2O_2 production. However, owing to the non-conductivity of PTFE, excessive hydrophobicity of the carbon materials not only hinders the electron transfer, but also impedes the hydrophilic mass transfer of H^+ and H_2O_2 on the surface of the carbon material, which leads to the inhibition of the catalytic reduction of oxygen. Moreover, because the O_2 reduction reaction is hydrophilic, a single hydrophobic modification of carbon materials is not conducive to the catalytic reduction of O_2 [33]. In this case, the synergistic regulation of the hydrophilicity/hydrophobicity of carbon materials to simultaneously enhance the diffusion adsorption and catalytic reduction of O_2 is highly desired.

To further enhance electron transfer in O_2 reduction, hydrophilic modification of the carbon material is indispensable. Some studies have shown that transition metal oxides, owing to their hydrophilicity and unique d-band center, can form highly active catalytic sites on the surface of carbon materials, thereby improving the synthesis efficiency of H_2O_2 [34–38]. ZrO_2 has excellent potential for hydrophilic modification of carbon materials to produce H_2O_2 because of its Brønsted surface sites and abundant hydrophilic oxygenated groups [39,40]. In addition, the modification of ZrO_2 can increase the electrochemically active surface area of carbon [41,42]. The modification of mesoporous carbon with ZrO_2, thus exhibits great potential for enhancing the hydrophilic catalytic activity of the cathodes.

Furthermore, since the hydrophobicity of O_2 leads to its low solubility in water (~0.5 mmol·L^{-1} at 25 °C and 0.1 MPa atmospheric pressure) and the traditional immersed flat electrode can only capture dissolved oxygen [43], a delay occurs in the ORR kinetics, which greatly limits the H_2O_2 yield. Under these circumstances, the adoption of cathodic gas-diffusion chamber is of great significance for enhancing O_2 mass transfer. Oxygen is flushed through the hydrophobic layer of the cathode, which can directly strengthen the diffusion and adsorption of O_2 in carbon pores and effectively improve the oxygen utilization efficiency [44].

Therefore, a systematic solution for the efficient *in situ* generation of H_2O_2 and its application to refractory organic degradation was proposed based on the fabrication of a novel ZrO_2/CMK-3/PTFE cathode, as shown in Fig. 1: ① PTFE, as an excellent hydrophobic material, was used to modify the macroporous carbon cathode material (carbon paper, CP) to form a superhydrophobic layer, aimed at improving the O_2 mass transfer and enhancing its adsorption and enrichment in the mesoporous carbon CMK-3; ② ZrO_2 modified CMK-3 was coated on the other side of the cathode as a hydrophilic catalytic layer, aiming to strengthen the hydrophilic catalytic reduction of O_2 and further enhance the electron transfer; and ③ a cathodic gas-diffusion chamber, with O_2 flowing through the hydrophobic layer of the cathode, was adopted to further improve the O_2 mass transfer in the mesoporous carbon. Thus, a mesoporous carbon gas-diffusion cathode (ZrO_2/CMK-3/PTFE) with efficient O_2 mass transfer and high catalytic reduction activity was constructed. The influence of the synergy between ZrO_2, CMK-3, and PTFE on H_2O_2 production was explored, and the relationships between H_2O_2 generation performance and O_2 mass transfer, electron transfer, electrolyte pH, and stability were established. The O_2 mass transfer limitation of ZrO_2/CMK-3/PTFE was also evaluated and compared with that of a conventional GDE. The results indicated a high H_2O_2 generation rate, 7.56 times higher than that of common GDE under the same conditions. High H_2O_2 yield (125.89 mmol·g^{-1}·h^{-1}) and Faraday efficiency (FE) (78.24%) were realized even at an industrial-relevant current of −252 mA·cm^{-2}. The EF activity of the ZrO_2/CMK-3/PTFE was explored through the degradation and mineralization of rhodamine B (RhB), methyl orange (MO), methylene blue (MB), and phenol in a flow-type cyclic degradation system. This study offers a novel engineering solution for the efficient treatment of refractory organic wastewater using EF technology based on the *in situ* high-yield H_2O_2 generation.

2. Experimental section

2.1. Chemicals and materials

All chemicals used in this study were of analytical grade and used without further purification. Mesoporous carbon CMK-3 (XFNANO, China), ZrO_2 (99.99% metals basis, particle size ≤ 100 nm; Aladdin, China), PTFE dispersions (Macklin, China), CP (Shanghai Keqi, China) were used for ZrO_2/CMK-3/PTFE preparation. Nafion 117 membrane and Nafion PFSA-polymer dispersions were obtained from DuPont (USA). $FeSO_4·7H_2O$ was purchased from Sinopharm Chemical Reagent Co., Ltd. Sulfuric acid (H_2SO_4) and sodium hydroxide (NaOH) were used for pH adjustment. RhB was purchased from Macklin Group Co., Ltd. Ultrapure water (≥18.25 MΩ·cm) utilized for the preparation/dilution of all samples was produced by the Milli-Q UP water system (Millipore, USA).

2.2. Fabrication of ZrO_2/CMK-3/PTFE electrode

A schematic of the ZrO_2/CMK-3/PTFE electrode fabrication process is shown in Fig. 1(a). After ultrasonic cleaning with ultrapure water, ethanol, and ultrapure water (in sequence) for 30 min, the cleaned CP was immersed in the PTFE suspension (2%, v/v) for 10 min, taken out and dried in an oven, and calcined at 360 °C
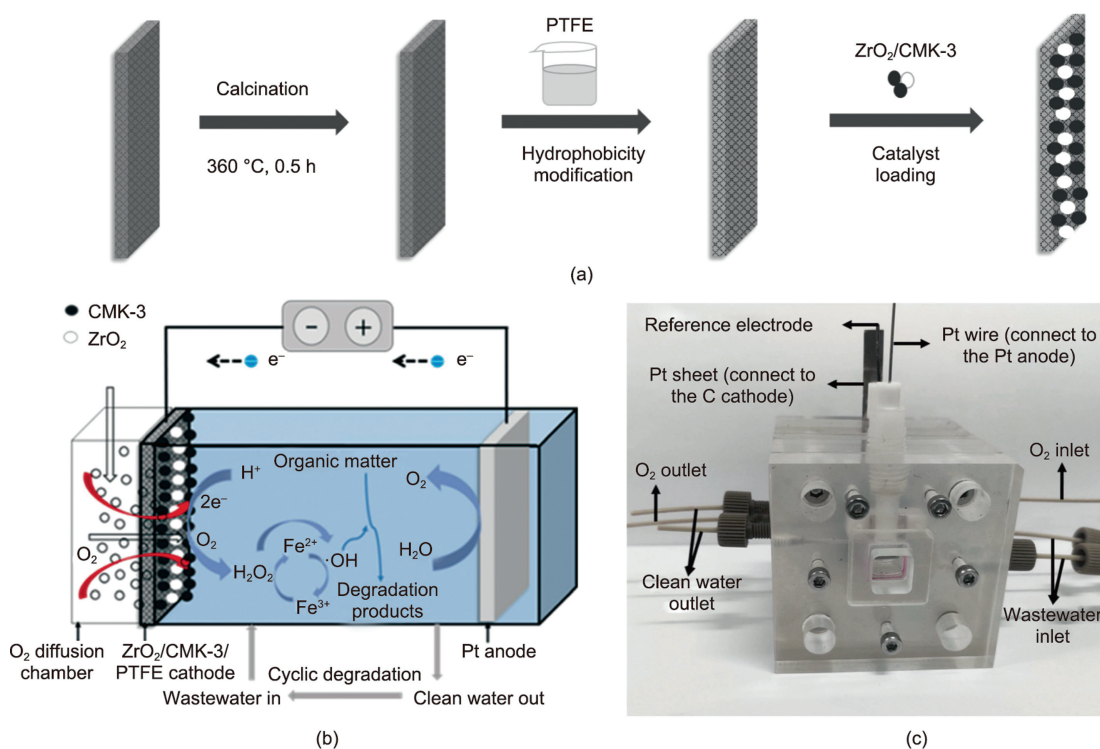
Fig. 1. (a) The fabrication process of the ZrO$_2$/CMK-3/PTFE cathode. (b) Schematic illustration and (c) photograph of the electrochemical reactor system for wastewater remediation.

for 30 min to form a superhydrophobic layer [28]. The catalyst suspension was prepared as follows: 40 mg CMK-3 catalyst, 80 mg ZrO$_2$, 2 mL ultrapure water, 10 mL ethanol, and 250 μL Nafion solution (5 wt%) were mixed by sonication. Subsequently, the catalyst suspension (2 mL) was spray-coated on the other side of the commercial CP (235 μm thick) to obtain a catalytic layer with a CMK-3 catalyst loading of 0.653 mg·cm^{-2}. Finally, the electrode loaded with the catalytic layer was calcined in a muffle furnace at 360 °C for 0.5 h and allowed to cool down for later use.

2.3. Characterization of electrode

The surface micromorphology and composition of the ZrO$_2$/CMK-3/PTFE electrode were characterized using field-emission scanning electron microscopy (FE-SEM; Ultra Plus, Zeiss, Germany) with an energy dispersive spectrometer (EDS). Contact angle (CA) measurements were conducted using a drop shape analyzer (DSA 100, KRUSS, Germany). Fourier-transform infrared (FT-IR) spectra were recorded between 4000 and 400 cm^{-1} using a Thermo Nicolet 6700 spectrometer (Thermo Fisher, USA). The crystal structure was characterized using X-ray diffraction (XRD; AXS-8 Advance; Bruker, Germany). The elemental compositions and states were analyzed using X-ray photoelectron spectroscopy (XPS; AXIS Ultra DLD; Kratos, Japan) with an Al Kα source (1486.6 eV, 1 eV = 1.602176 × 10^{-19} J). Electron spin resonance (ESR) spectra were measured using electron paramagnetic resonance spectrometer (EPR 300E, Bruker).

2.4. Electrochemical measurement and analysis

All electrochemical measurements were performed on a CHI660D electrochemical workstation (CH Instruments Inc., USA) using a three-electrode system [45]. Linear sweep voltammetry (LSV) measurements were performed at a scan rate of 50 mV·s^{-1}. A ZrO$_2$/CMK-3/PTFE electrode (1 cm × 1 cm) was used as the working electrode, and a Pt sheet (1.0 cm × 1.5 cm) and Ag/AgCl

electrode were used as the counter and reference electrodes, respectively. All electrochemical measurements were performed in a 0.1 mol·L^{-1} Na$_2$SO$_4$ electrolyte solution with pH of 1–7. The measured potentials versus Ag/AgCl electrode were converted to the standard hydrogen electrode (SHE) scale according to the Nernst formula:

$$E_{SHE} = E_{Ag/AgCl} + 0.1976 \qquad (3)$$

where E_{SHE} represents the converted potential versus SHE and $E_{Ag/AgCl}$ is the applied potential versus Ag/AgCl.

Electrocatalytic H$_2$O$_2$ production on the ZrO$_2$/CMK-3/PTFE electrode was performed in a flow-through cell reactor with three chambers (cathodic chamber, anodic chamber, and O$_2$ diffusion chamber), as shown in Fig. 1(c) and Fig. S1 in Appendix A. Each chamber contained a cavity (1 cm × 1 cm × 1 cm) and channels (0.2 mm diameter) for electrolyte or O$_2$ delivery. The cathodic and anodic chambers were separated using a Nafion 117 membrane (1 cm × 1 cm). The gas diffusion cathode was assembled tightly between the cathode chamber and O$_2$ diffusion chamber with the catalytic layer facing the electrolyte and the gas diffusion layer facing O$_2$. A Pt sheet (1.0 cm × 1.5 cm) was placed 2.5 cm away from the gas diffusion cathode in parallel and used as the anode in all electrolytic experiments. A Pt wire and Pt sheet were used to connect the anode and cathode, respectively. Adjacent chambers were sealed with elastic silicone gaskets. The anodic and cathodic chambers were filled with the same electrolyte.

For the quantitative analysis of generated H$_2$O$_2$, samples were collected at certain time intervals, and analyzed using the potassium titanium oxalate method [20], and measured using an ultraviolet (UV)–visible (Vis) spectrophotometer (752 N, INESA, China) at a maximum absorption wavelength of 410 nm. The FE (%) of the H$_2$O$_2$ synthesis was calculated using Eq. (4):

$$FE = \frac{nCVF}{\int_0^t Idt} \qquad (4)$$

where n is the transferred electron number (for H_2O_2, $n = 2$), C is the H_2O_2 concentration (mol·L^{-1}), V is the volume of the electrolyte solution (L), F is the Faraday constant (C·mol^{-1}), I stands for the current passing through the cathode (mA), and t is the time (s).

The EF degradation of contaminants was conducted in 0.1 mol·L^{-1} Na_2SO_4 containing 1 mmol·L^{-1} Fe^{2+}, and the initial pH was adjusted to 4 using H_2SO_4. The initial concentration of RhB was 100 mg·L^{-1}, whereas the concentration was 20 mg·L^{-1} for the other contaminants. The reactor and electrodes were the same as those used for H_2O_2 production unless otherwise mentioned. The concentrations of RhB, MO, MB, and phenol were analyzed by UV–vis spectrophotometry at characteristic wavelengths of 552, 465, 662, and 270 nm, respectively. Total organic carbon (TOC) was determined using a TOC/total nitrogen (TN) analyzer (multi N/C 3100, Analytik Jena, Germany) to investigate the degree of mineralization. The pollutant degradation efficiency (η) following the UV measurements was calculated using Eq. (5):

$$\eta = \frac{C_0 - C_t}{C_0} \times 100\% \tag{5}$$

where C_0 and C_t (mg·L^{-1}) are the initial and final pollutant concentrations, respectively.

TOC removal efficiency (δ) was calculated using Eq. (6):

$$\delta = \frac{TOC_0 - TOC_t}{TOC_0} \times 100\% \tag{6}$$

where TOC_0 and TOC_t (mg·L^{-1}) are the initial and final TOC contents of the pollutants, respectively. To check reproducibility, all runs were repeated at least three times.

3. Results and discussions

3.1. Fabrication and characterization of ZrO_2/CMK-3/PTFE

The small thickness and asymmetric hydrophilic/hydrophobic characteristics of the alveolar membrane in organisms enable oxygen to pass through the alveolar membrane to achieve efficient mass transfer [31]. Inspired by this, a dual-modified gas-diffusion cathode with a hydrophilic/hydrophobic interface was designed in this study and referred to as ZrO_2/CMK-3/PTFE. In this, PTFE was used as a hydrophobic modifier to improve oxygen mass transfer and ZrO_2 was used as a hydrophilic modifier to enhance the production and mass transfer of H_2O_2 because of its abundant hydrophilic oxygen-containing functional groups. As shown in Fig. 1, the PTFE-modified CP acted as a matrix and gas diffusion layer, while the ZrO_2-decorated CMK-3 was coated on the other side to form the ZrO_2/CMK-3/PTFE electrode. As shown in the SEM images, CMK-3 consists of amorphous carbon with ZrO_2 uniformly distributed on it (Fig. 2(a)). The CP consisted of a macroporous backing material (interconnected carbon fiber) and a microporous carbon-based layer (Figs. 2(b) and (c)). The small thickness (∼235 μm) and porous structure of the CP endow it with a high gas diffusion performance (Fig. 2(d)), which can greatly reduce the oxygen diffusion resistance and prevent the occurrence of water flooding to improve the durability of the electrode. The surface hydrophobicity of CP was assessed using water CA measurements. As shown in Fig. 2(c), the PTFE-modified CP exhibited excellent hydrophobicity with a water CA of 144.2°, indicating superior water resistance to promote the diffusion of molecular
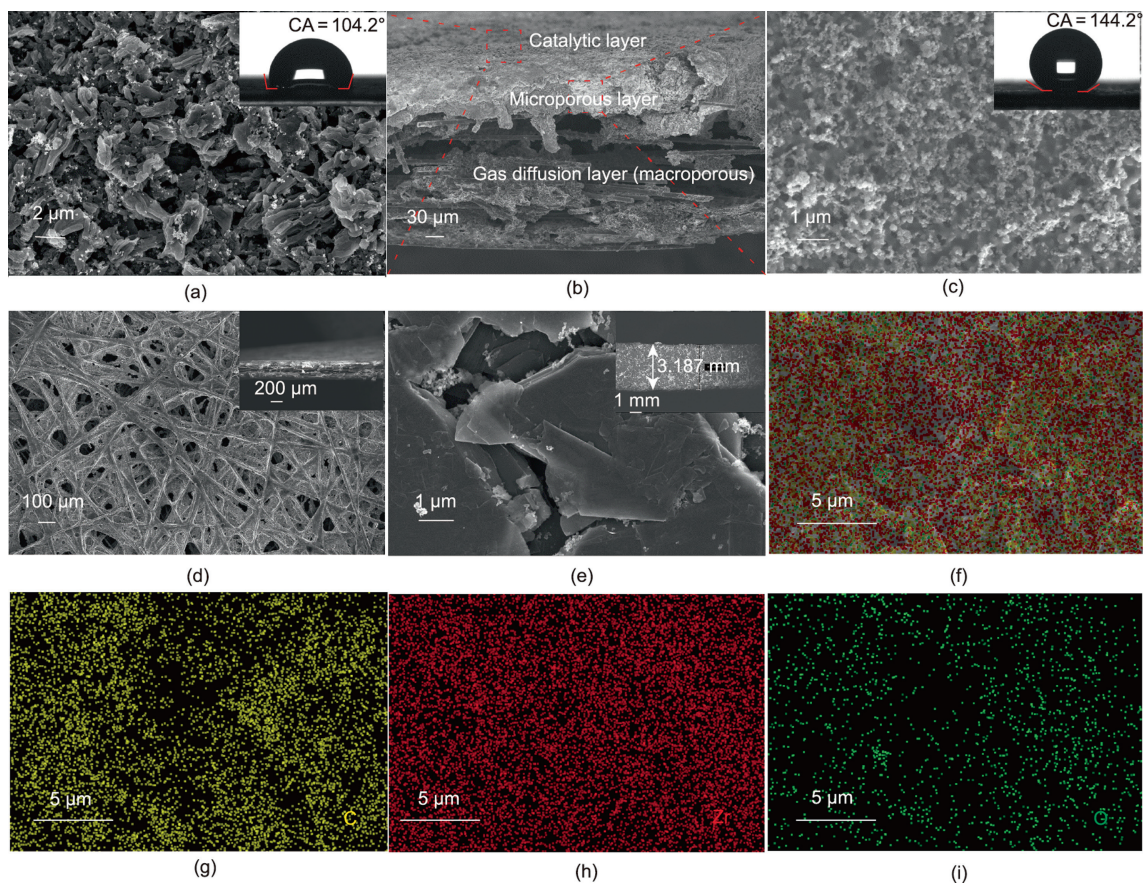

Fig. 2. (a) SEM image and CA (insert) of the CP substrate coated with ZrO_2/CMK-3. (b) Cross-sectional SEM image of ZrO_2/CMK-3 catalysts on CP. (c) SEM image and CA (insert) of PTFE-modified CP. SEM images of (d) the back of CP and (e) conventional GDE (insert is the cross-sectional view). (f) EDS elemental mapping images of ZrO_2/CMK-3: (g) C, (h) Zr, and (i) O.

oxygen to the catalyst layer. In contrast, the catalytic layer showed a relatively small CA of 104.2° (Fig. 2(a)), demonstrating that the catalyst side has more hydrophilic characteristics that promote the transfer of $2e^-$ – ORR products. With a Janus structure and short gas diffusion length, the prepared gas diffusion cathode can provide sufficient gas–liquid–solid three-phase contact for the efficient diffusion of O_2 and rapid transfer of the water-soluble product H_2O_2. Comparably, the conventional GDE features a relatively thick and dense pore structure, which is not conducive to oxygen mass transfer (Fig. 2(e)). Therefore, by producing the same amount of H_2O_2, the proposed ZrO_2/CMK-3/PTFE cathode has better energy efficiency for oxygen diffusion than the traditional GDE, this is more beneficial for cost-effective applications.

The SEM image (Fig. 2(a)) clearly shows that the catalytic layer of the ZrO_2/CMK-3/PTFE electrode has a loose skeleton and an interconnected porous structure. In addition, the EDS mappings shown in Figs. 2(f)–(i) demonstrate the existence and uniform dispersion of C, Zr, and O in the selected architecture. X-ray photoelectron spectroscopy was used to further analyze the surface elemental compositions and chemical bonding states of the ZrO_2/CMK-3 catalyst. The results are shown in Fig. 3. The survey spectrum shows several strong peaks assigned to C 1s, O 1s, and Zr 3d, indicating a catalyst layer composed of C and ZrO_2 (Fig. 3(a)). The C 1s spectra displayed a variety of components corresponding to sp^2 C–C bonds (~284.5 eV), C–H bonds (~285.0 eV), epoxy C–O bonds (~286.0 eV), carbonyl C=O bonds (~288.2 eV), and carboxyl O–C=O bonds (~290.0 eV) (Fig. 3(b)) [39,46]. The additional component at 291.9 eV may be related to the photoemission-induced plasmonic $\pi \rightarrow \pi^*$ transitions [47]. The O 1s spectra were deconvo-

luted into four independent peaks at 530.3, 531.0, 532.0, and 533.1 eV corresponding to O–Zr (derived from nano-ZrO_2 embedded in the carbon material), carbonyl groups (O=C), alcohols groups (C–O), and carboxyl groups (O–C=O), respectively (Fig. 3(c)). In the Zr 3d region (Fig. 3(d)), the spectrum had two independent peaks at 182.7 and 185.0 eV, and the interval was 2.3 eV, consistent with the standard ZrO_2 spectrum [39].

3.2. Electrocatalytic activity of ZrO_2/CMK-3/PTFE

To explore the electrosynthesis efficiency of H_2O_2 on the ZrO_2/CMK-3/PTFE cathode, H_2O_2 yield and FE were evaluated. In this study, the electrodes were immersed in an electrolyte solution, and oxygen was diffused through the electrolyte to the cathode surface (normal aeration). For comparison, a series of electrodes were prepared: pure CP, CMK-3 (CMK-3 supported on pure CP), CMK-3/PTFE (CMK-3 supported on PTFE-modified CP), and ZrO_2/CMK-3 (ZrO_2/CMK-3 supported on pure CP). As shown in Fig. 4 (a), the H_2O_2 production rate and FE at the different cathode interfaces displayed significant differences. The yield of H_2O_2 at the ZrO_2/CMK-3/PTFE cathode reached the maximum (1.21 mg·cm^{-2}·h^{-1}), which was approximately 2.42 times that at the CMK-3 cathode (0.50 mg·cm^{-2}·h^{-1}) and 1.92 times that at the ZrO_2/CMK-3 cathode (0.63 mg·cm^{-2}·h^{-1}). Meanwhile, the FE of the ZrO_2/CMK-3/PTFE cathode reached 56.3%, which was 12.3% and 11.3% higher than those of the CMK-3 (44%) and ZrO_2/CMK-3 cathodes (45%), respectively. The LSV plots of the different cathodes were obtained to assess the ORR activity of the catalytic layer (Fig. 4(b)). As the cathode potential shifted negatively, the current response
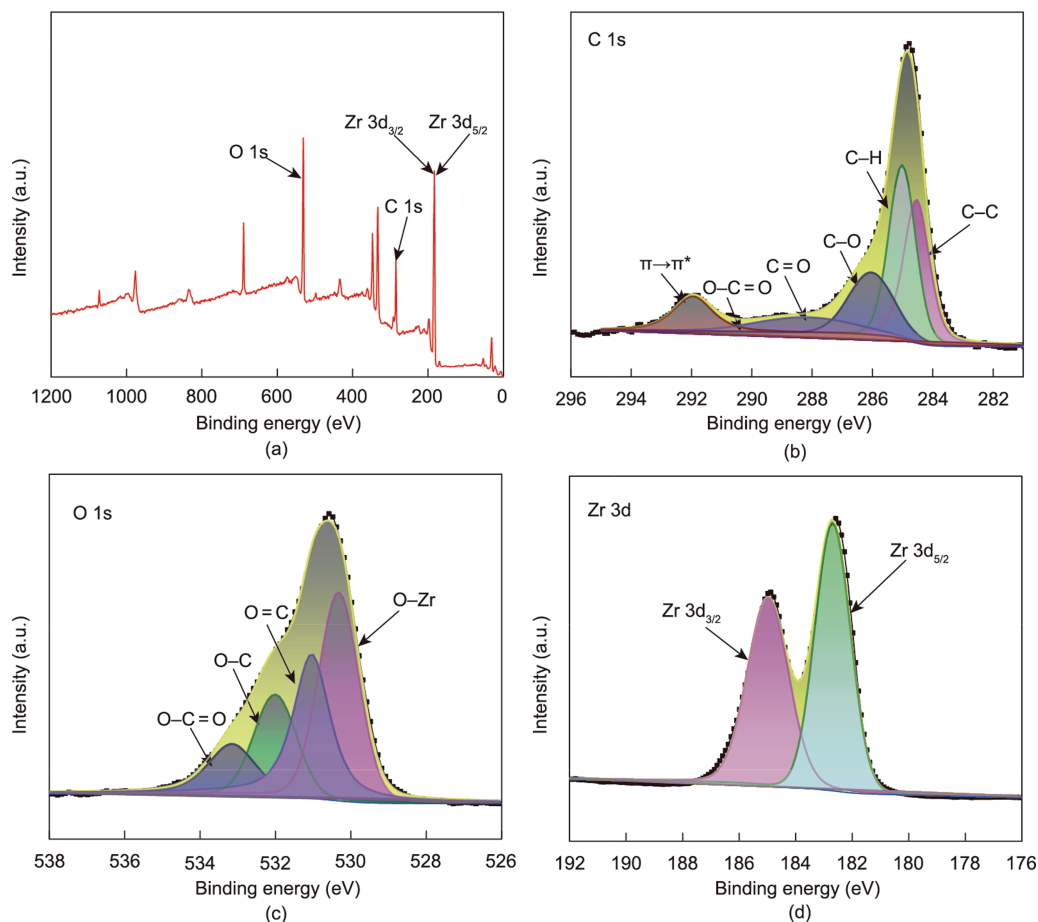

Fig. 3. (a) XPS survey spectra, (b) C 1 s, (c) O 1 s, and (d) Zr 3d of the ZrO_2/CMK-3/PTFE electrode.

increased gradually. The current response of the CMK-3 cathode was significantly improved by the synergistic modification of ZrO_2 and PTFE, suggesting that ZrO_2 and PTFE have a synergistic effect on improving the H_2O_2 production performance of the CMK-3 cathode. As discussed in Section 2.2, the PTFE treatment could form superhydrophobic layer on the electrode surface, which is conducive to the diffusion of oxygen to the surface of the catalytic layer for the reduction reaction [48]. However, the excessive hydrophobicity of the electrode surface may inhibit the transfer of H^+ from the electrolyte to the electrode surface and the mass transfer of H_2O_2 in the opposite direction [49]. Moreover, the nonconductive properties of PTFE may increase the Ohmic polarization of the electrode, and the increase in electrode resistance causes difficulties in electron transport, thereby suppressing the $2e^-$ – ORR performance of the electrode [50]. To maintain the hydrophilic/hydrophobic balance of the three-phase structure of the electrode, an appropriate adjustment in the hydrophilicity of the PTFE-modified electrode appears to be significant. For this purpose, we employed a Nafion solution as a binder to mix mesoporous carbon CMK-3 and ZrO_2 and sprayed it on the other side of the electrode using a spray method. Owing to the presence of both acidic and basic sites on its surface [51], ZrO_2 induced more oxygenated functional groups (such as C–OH, C=O, C–OOH, and C–O–C) on the surface of CMK-3, resulting in high surface hydrophilicity and the accelerated formation of a gas–liquid–solid three-phase interface on the electrode surface, as confirmed by XPS and FT-IR (Fig. 3 and Fig. S2 in Appendix A). Moreover, the existence of oxygenated functional groups can greatly promote the $2e^-$ oxygen reduction activity of the electrode, and the C=O species, in particular, contribute most to the electrocatalytic activity and are the most active sites [52]. Combining the above analysis and XPS results, it can be demonstrated that the excellent H_2O_2 production ability of the

ZrO_2/CMK-3/PTFE electrode should be ascribed to the existence of considerable oxygenated functional groups (particularly C=O) on the electrode catalytic layer. In addition, as a mesoporous carbon material, CMK-3 has excellent electrical conductivity, and its combination with ZrO_2 can strengthen the electron conduction rate and enhance the oxygen reduction performance of the electrode. Nafion is a hydrophilic resin that can act as a binder to enhance the wettability of the electrode surface. Nafion is also an excellent proton conductor that can improve the proton transport in the catalyst and promote the reaction of protons and oxygen on the electrode surface [50].

Because the increased CMK-3:ZrO_2 mass ratio led to an increase in the ZrO_2 mass and thus provided additional oxygenated functional group active sites per unit mass of carbon, a higher H_2O_2 yield on the ZrO_2/CMK-3/PTFE electrode could be achieved. Accordingly, the influence of different CMK-3:ZrO_2 mass ratios on the H_2O_2 yield and FE of the ZrO_2/CMK-3/PTFE electrode needs to be investigated. The CMK-3:ZrO_2 mass ratio was studied in the range 1.0:0.5–1.0:4.0. The results are displayed in Figs. 4(c) and (d), which show that when the mass ratio of CMK-3:ZrO_2 was 1.0:0.5, the H_2O_2 production rate reached 0.88 mg·cm^{-2}·h^{-1} in 60 min. As the proportion of ZrO_2 increased, the H_2O_2 production rate increased significantly. When the ratio was increased to 1.0:2.0, the production of H_2O_2 reached its highest value (1.21 mg·cm^{-2}·h^{-1}). However, as the mass ratio of CMK-3:ZrO_2 was further increased to 1.0:4.0, the H_2O_2 production decreased (0.76 mg·cm^{-2}·h^{-1}).The electrode with a CMK-3:ZrO_2 mass ratio of 1.0:2.0 reached the highest FE (56.3%), and this trend was consistent with that for H_2O_2 yield. Compared to the CP and CMK-3/PTFE electrodes, the XRD pattern of the ZrO_2/CMK-3/PTFE electrode showed apparent characteristic peaks of ZrO_2 (Fig. 4(e)). In addition, as expected, the XRD patterns of the ZrO_2/CMK-3/PTFE
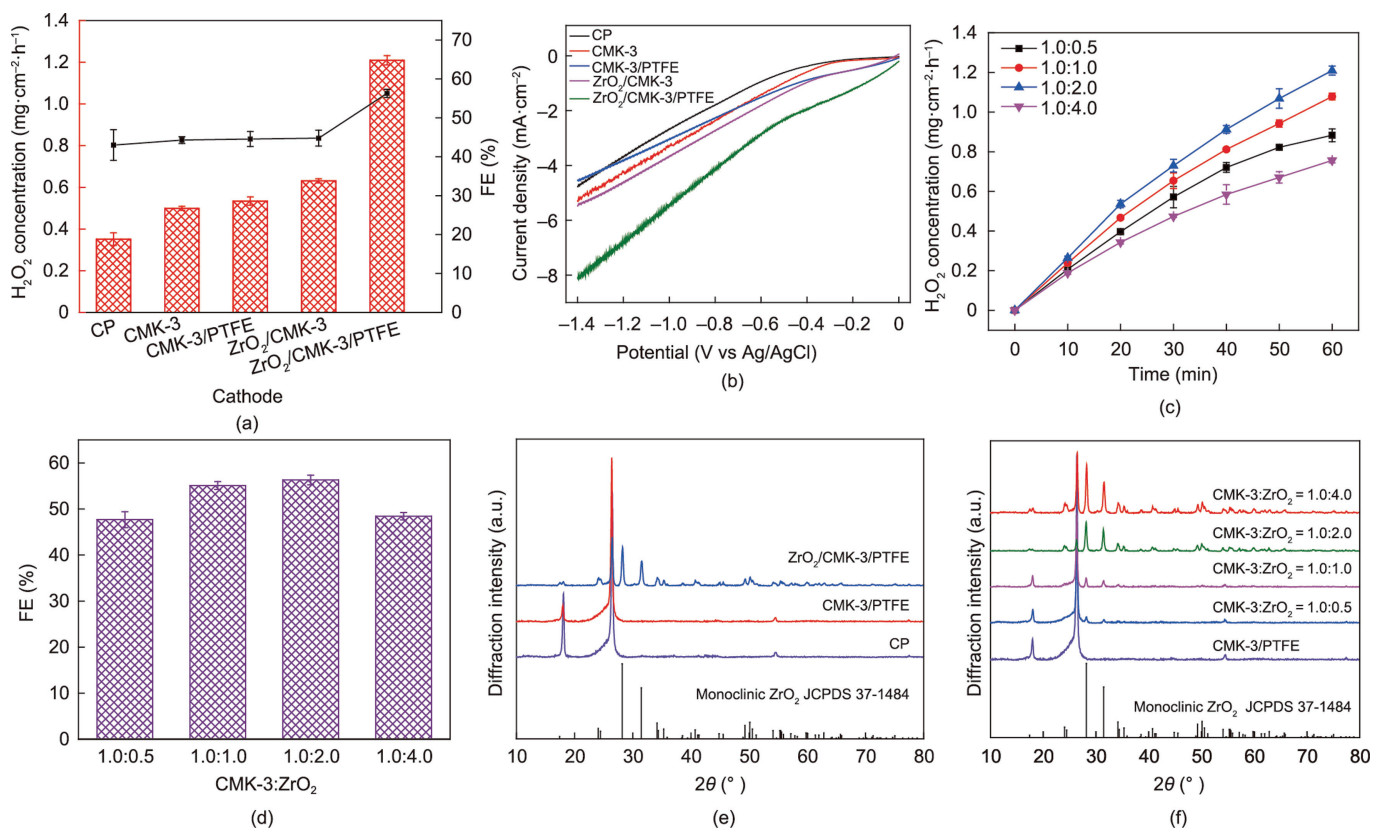

Fig. 4. (a) H_2O_2 yield and FE, (b) LSV curves of different carbon electrodes. (c) H_2O_2 generation, (d) FE of ZrO_2/CMK-3/PTFE with different CMK-3:ZrO_2 mass ratios. XRD patterns of (e) different carbon electrodes and (f) ZrO_2/CMK-3/PTFE with different CMK-3:ZrO_2 mass ratios. Conditions: pH = 4, −0.5 V vs SHE, and normal aeration.

electrode with different CMK-3:ZrO$_2$ mass ratios showed that the mass of ZrO$_2$ and its characteristic peak intensity also changed (Fig. 4(f)). The cathode with increased ZrO$_2$ content also displayed a more hydrophilic CA, as shown in Appendix A Fig. S3. When the mass ratios of CMK-3:ZrO$_2$ were 1.0:0, 1.0:0.5, 1.0:1.0, and 1.0:4.0, the CAs were 131.3°, 127.6°, 116.5°, and 96.5°, respectively. Because the increased ZrO$_2$ mass increased the number of oxygenated functional group active sites, the production of H$_2$O$_2$ increased. The increase in ZrO$_2$ mass also increases the hydrophilicity of the electrode surface, which can easily cause the electrolyte to penetrate the electrode and cause water flooding [44]. In addition, excessive nano-ZrO$_2$ content is prone to agglomeration, which causes a sharp decrease in the micropores and specific surface area, narrowing the oxygen transport channel and does not promote the progress of the ORR.

3.3. Performance comparison with other cathodes

Because GDE has been extensively studied to improve oxygen mass transfer to obtain better H$_2$O$_2$ production [21,53], the H$_2$O$_2$ production of the ZrO$_2$/CMK-3/PTFE cathode and the traditional GDE fabricated by the rolling method was compared. The electrodes were immersed in the electrolyte solution and oxygen diffused through the electrolyte to the cathode surface. As presented in Fig. 5(a), H$_2$O$_2$ yield on ZrO$_2$/CMK-3/PTFE cathode at potential of −0.5 V versus SHE was 1.21 mg·cm^{-2}·h^{-1}, which was 7.56 times that of the traditional GDE (0.16 mg·cm^{-2}·h^{-1}). The traditional GDE had a FE of 30.3%, while that of the ZrO$_2$/CMK-3/PTFE cathode was 56.3% (Fig. 5(b)). The performance of the traditional GDE was consistent with previous reports [49]. The relatively large thickness and dense pore structure of the conventional GDE (Fig. 2(e)) impeded oxygen mass transfer, which resulted in a decrease in H$_2$O$_2$ production efficiency. The H$_2$O$_2$ production performances of the Pt electrode and ZrO$_2$ and PTFE-modified acetylene black (AB) electrodes (ZrO$_2$/AB/PTFE) were also compared. The Pt electrode (0.011 mg·cm^{-2}·h^{-1}) and ZrO$_2$/AB/PTFE cathode (0.45 mg·cm^{-2}·h^{-1}) exhibited relatively low H$_2$O$_2$ yields, which were 1/110.00 and 1/2.69 of the ZrO$_2$/CMK-3/PTFE cathode, respectively. Moreover, the ZrO$_2$/CMK-3/PTFE cathode maintained stable H$_2$O$_2$ production efficiency and FE even after using it 10 times (10 h, as displayed in Appendix A Fig. S4); this is exceptional H$_2$O$_2$ production performance. Owing to its ordered mesoporous structure, CMK-3 exhibited reasonable selectivity and potential scalability for H$_2$O$_2$ generation [54]. Consequently, the excellent performance of the prepared cathode can be ascribed not only to the hydrophilic/hydrophobic Janus structure, which ensured rapid

mass transfer of O$_2$ and H$_2$O$_2$, but also to the sufficient number of active sites, which ensured excellent 2e$^-$ − ORR selectivity.

3.4. Effect of hydrophobic diffusion of O$_2$ on H$_2$O$_2$ production

After demonstrating the extraordinary H$_2$O$_2$ production performance of the ZrO$_2$/CMK-3/PTFE electrode, it is highly desirable to investigate the effect of the hydrophobic diffusion modes of O$_2$ on H$_2$O$_2$ production. We compared H$_2$O$_2$ production and FE of the proposed cathode using different aeration modes. In gas diffusion aeration, the hydrophobic layer of the ZrO$_2$/CMK-3/PTFE cathode faced continuous O$_2$ flow, and the 2e$^-$ − ORR proceeded in the electrolyte solution on the other side of the cathode. Under normal aeration, the cathode is immersed in the electrolyte solution and can only trap dissolved oxygen from the solution. As shown in Fig. 6(a), the production of H$_2$O$_2$ through gas diffusion aeration increased significantly, reaching 4.47 mg·cm^{-2}·h^{-1}, which is 3.7 times that of normal aeration (1.21 mg·cm^{-2}·h^{-1}). The FE of H$_2$O$_2$ generated by gas diffusion aeration was 91.84%, which was 35.57% higher than that under normal aeration (56.27%). Moreover, as shown by the LSV (Fig. 6(b)) and current density–time (J–t) curves (Fig. 6(c)), the current density of the ZrO$_2$/CMK-3/PTFE cathode system in gas diffusion aeration was significantly higher than that in normal aeration mode. This is mainly because the normal aeration mode is limited by the oxygen mass transfer, leading to less ORR activity. The gas diffusion aeration mode creates a triple-phase interface for the catalytic reaction and reduces the mass transport limitation caused by the poor solubility of O$_2$ in water [55]. Thus, the gas diffusion design enables the electrochemical reaction cell to operate at high current densities and realizes efficient H$_2$O$_2$ production.

The excellent H$_2$O$_2$ production performance of the ZrO$_2$/CMK-3/PTFE electrode was verified by testing the actual amount of H$_2$O$_2$ generated under varying potential and solution pH values. As shown in Fig. 7(a), when O$_2$ was electrochemically reduced on ZrO$_2$/CMK-3/PTFE electrode at pH 1, the production rate of H$_2$O$_2$ was 30.32–125.98 mg·cm^{-2}·h^{-1} at the potential of −0.3 to −1.3 V versus SHE (current density of −52 to −252 mA·cm^{-2}). Meanwhile, ZrO$_2$/CMK-3/PTFE gave a high mass yield for H$_2$O$_2$ production, and the corresponding H$_2$O$_2$ generation rate normalized by the catalyst loading was 1365.78–5674.04 mmol·g^{-1}·h^{-1} on ZrO$_2$/CMK-3/PTFE at a potential between −0.3 and −1.3 V versus SHE. Notably, the H$_2$O$_2$ yield increased as the potential shifted negatively within the investigated potential range. The varying H$_2$O$_2$ yield followed the same trend at pH 4 and 7. The H$_2$O$_2$ production rate increased from 3.03 mg·cm^{-2}·h^{-1} (−0.3 V) to 11.74 mg·cm^{-2}·h^{-1}
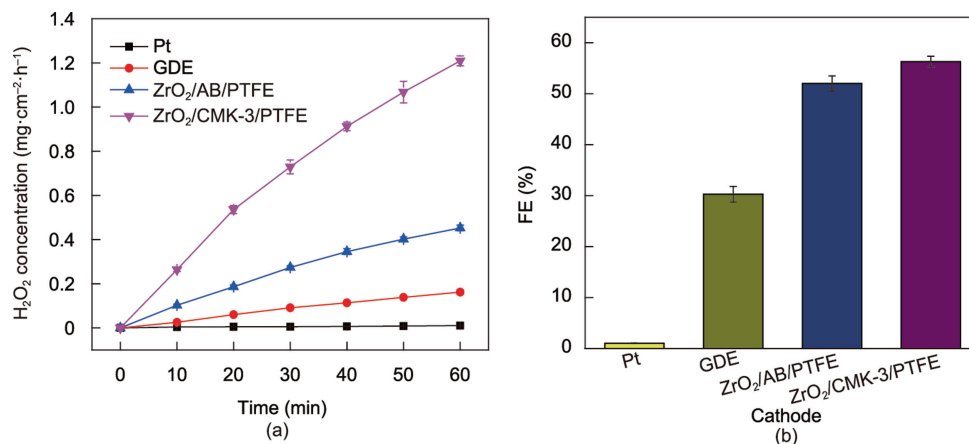

Fig. 5. Comparison of (a) H$_2$O$_2$ yield and (b) FE for the ZrO$_2$/CMK-3/PTFE with other cathodes. Conditions: pH = 4, −0.5 V vs SHE, and normal aeration.
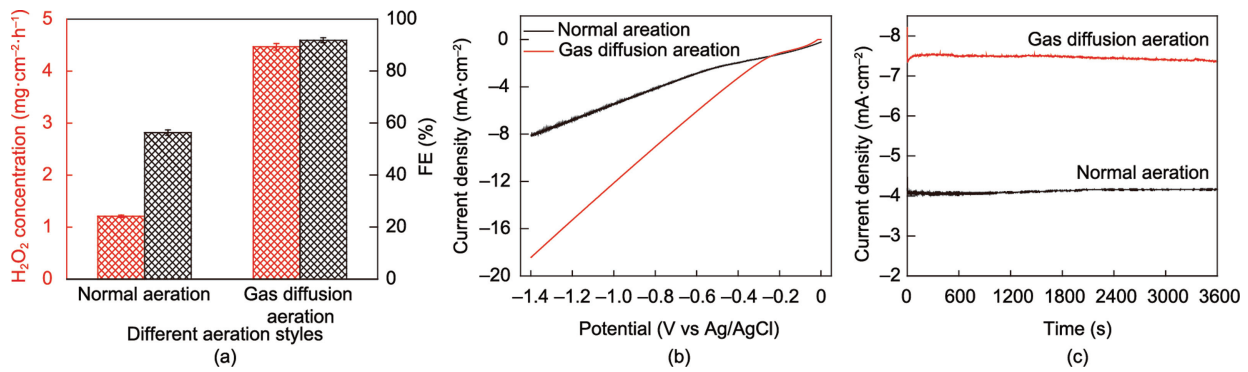
Fig. 6. Effects of (a) aeration styles on H_2O_2 generation and FE, (b) current density of ZrO_2/CMK-3/PTFE. (c) The J–t curve of H_2O_2 electrosynthesis for 1 h. Conditions: pH = 4, −0.5 V vs SHE.
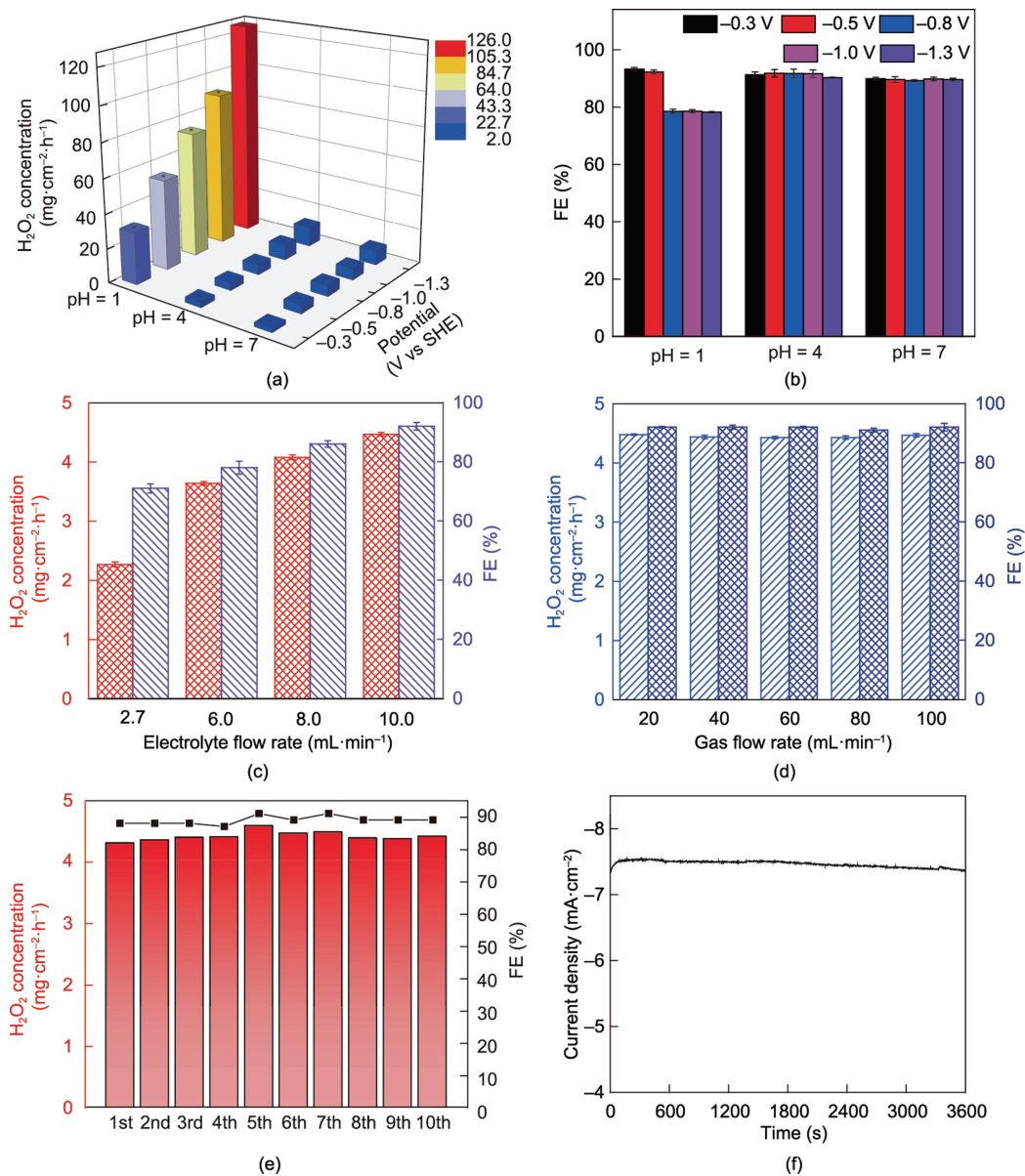

Fig. 7. (a) H_2O_2 production and (b) FE of ZrO_2/CMK-3/PTFE at pH 1–7 and potential of −0.3 to −1.3 V vs SHE. Effect of (c) electrolyte flow rate and (d) O_2 flow rate on H_2O_2 production and FE. (e) The stability test of the ZrO_2/CMK-3/PTFE used for H_2O_2 generation in 10 times continuous runs and (f) the J–t curve. Conditions: pH = 4, −0.5 V vs SHE, and gas diffusion aeration.

$(-1.3 \text{ V}, 528.68 \text{ mmol} \cdot \text{g}^{-1} \cdot \text{h}^{-1})$ at pH 4, and from $2.49 \text{ mg} \cdot \text{cm}^{-2} \cdot \text{h}^{-1}$ (-0.3 V) to $8.58 \text{ mg} \cdot \text{cm}^{-2} \cdot \text{h}^{-1}$ $(-1.3 \text{ V}, 392.37 \text{ mmol} \cdot \text{g}^{-1} \cdot \text{h}^{-1})$ at pH 7. At the same potential, a lower pH favored the production of H_2O_2 (consistent with previous studies [25,56]), which can be attributed to the participation of H^+ in the synthesis of H_2O_2. Nevertheless, $ZrO_2/CMK-3/PTFE$ exhibited high activity, even with a neutral solution. Compared with the cathodes in other studies, the $ZrO_2/CMK-3/PTFE$ cathode proposed in this study exhibited significant superiority in H_2O_2 yield and FE; the H_2O_2 yield increased by at least three times, and the H_2O_2 yield normalized to catalyst loading was improved by at least three orders of magnitude, as shown in Appendix A Table S1. These results indicate that $ZrO_2/CMK-3/PTFE$ cathode exhibits exceptional activity for H_2O_2 electrosynthesis over a wide range of potentials and pH values.

Because FE is an important indicator of electrocatalysis (EC) [57], the FE for H_2O_2 generation was also investigated to further evaluate the performance of $ZrO_2/CMK-3/PTFE$. As shown in Fig. 7(b), the FE at pH 1 was 78.24%–91.27% under a potential of -0.3 to -1.3 V versus SHE. Because the side reactions of H_2 evolution and H_2O_2 disproportionation could simultaneously occur on $ZrO_2/CMK-3/PTFE$, the yield and FE of H_2O_2 may decrease at high negative potentials and highly acidic pH [49]. As expected, $ZrO_2/CMK-3/PTFE$ retained a high FE (90.29%–91.84%) at pH 4. Interestingly, the FE in neutral solution also remained high (89.25%–89.95%). Although the FE decreased as the potential became increasingly negative, the performance was still satisfactory, which is essential and favorable for scaling up electrochemical devices from the laboratory scale to the industrial scale. Consequently, the above analysis indicated that $ZrO_2/CMK-3/PTFE$ exhibited remarkable H_2O_2 production performance, making it a promising cathode for wastewater treatment in H_2O_2-based electrochemical AOPs.

Considering that the flow rate of the electrolyte and O_2 may also influence H_2O_2 production, a series of experiments were conducted to investigate this. The results are depicted in Fig. 7(c): as electrolyte flow rate increased from 2.7 to 10.0 $\text{mL} \cdot \text{min}^{-1}$, H_2O_2 generation rate and FE also increased from 2.27 to 4.47 $\text{mg} \cdot \text{cm}^{-2} \cdot \text{h}^{-1}$, and 70.85% to 91.84%, respectively. Because a higher flow rate can replenish H^+ and transfer the product H_2O_2 faster, resulting in the reaction proceeding towards H_2O_2 production, a higher electrolyte flow rate exhibited higher H_2O_2 production and FE. Furthermore, even when the O_2 flow rate was decreased from 100 to 20 $\text{mL} \cdot \text{min}^{-1}$, the variations in the H_2O_2 generation rate (4.43–4.48 $\text{mg} \cdot \text{cm}^{-2} \cdot \text{h}^{-1}$) and FE (91.53%–92.37%) were negligible, and the ORR was not limited by oxygen mass transfer (Fig. 7(d)),

demonstrating that high H_2O_2 yield and FE can be achieved even with low oxygen supply in the proposed $ZrO_2/CMK-3/PTFE$ system.

Because the stability of the cathode is essential for practical applications [58], a stability test for $ZrO_2/CMK-3/PTFE$ cathode was conducted. As shown in Figs. 7(e) and (f), $ZrO_2/CMK-3/PTFE$ cathode exhibited excellent stability for H_2O_2 yield and FE during 10 consecutive H_2O_2 electrosyntheses (10 h). Additionally, compared to the cathode before an operation, the SEM image of the cathode after operation showed no significant change, and the hydrophobic interface of $ZrO_2/CMK-3/PTFE$ could still be maintained even after the EC for 10 h at the potential of -0.5 V versus SHE, (as presented in Appendix A Fig. S5). These results demonstrate the possibility of applying $ZrO_2/CMK-3/PTFE$ cathode for extended periods.

The outstanding electrocatalytic performance of the $ZrO_2/CMK-3/PTFE$ cathode can be attributed to the following factors: ① the PTFE-modified superhydrophobic substrate ensures the efficient and rapid mass transfer of molecular oxygen; ② the ordered mesoporous structure of CMK-3 endows it with abundant active sites and exhibits reasonable selectivity and potential scalability toward H_2O_2 generation; and ③ ZrO_2 adds a number of oxygenated functional groups on the CMK-3 surface, which strengthen the surface hydrophilicity and the conjunction of H_2O at the interface of the carbon cathode, thereby ensuring the efficient mass transfer of H^+ from the electrolyte to the catalytic layer and H_2O_2 from the catalytic layer to the electrolyte.

3.5. EF application for refractory organics degradation

Having demonstrated an extraordinary H_2O_2 production performance, the $ZrO_2/CMK-3/PTFE$ cathode's performance for successive EF degradation of organic pollutants deemed an evaluation. Accordingly, a flow-type cyclic degradation system was constructed, which was consistent with the one used for H_2O_2 production (as described in the Section 2.1), except for the absence of Nafion membrane separation (Fig. 1(c)). With efficient generation of H_2O_2 at the cathode and the circulating flow of wastewater, continuous and rapid EF degradation of organic pollutants could be realized (Fig. 1(b)). The results showed that at pH 4, 1.0 $\text{mmol} \cdot \text{L}^{-1}$ Fe^{2+}, and an applied potential of -0.3 V versus SHE, the degradation efficiency of the $ZrO_2/CMK-3/PTFE$ cathode system for 50 mL of 100 $\text{mg} \cdot \text{L}^{-1}$ RhB reached 82.9% at 30 min (Fig. 8(a)). The removal efficiencies of CP, CMK-3, CMK-3/PTFE, and $ZrO_2/CMK-3$ cathode systems for RhB were 7.1%, 51.2%, 57.1%, and 68.1%, respectively,
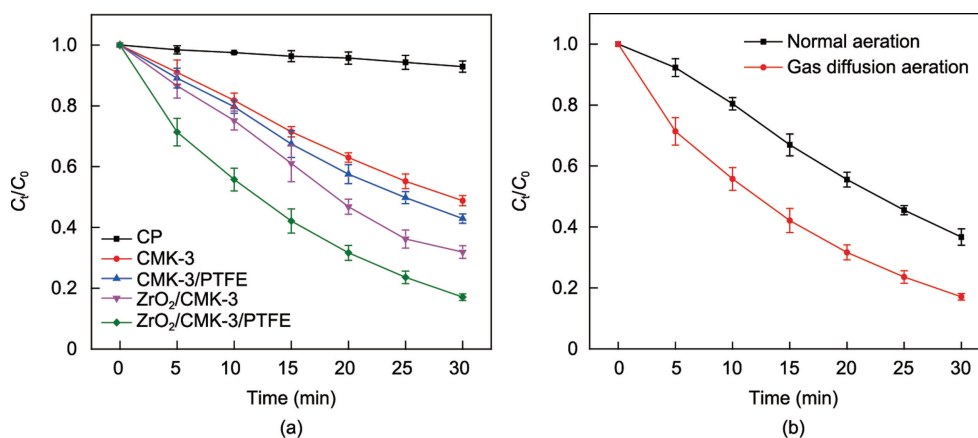

Fig. 8. (a) EF degradation efficiency of RhB on different cathodes. (b) Effect of different O_2 aeration styles on the degradation efficiency of RhB. Conditions: 100 $\text{mg} \cdot \text{L}^{-1}$ RhB, pH = 4, 1.0 $\text{mmol} \cdot \text{L}^{-1}$ Fe^{2+}, and -0.3 V vs SHE.

which were significantly lower than that of the ZrO_2/CMK-3/PTFE cathode system. Moreover, compared with normal aeration (63.3%), the gas diffusion aeration in the ZrO_2/CMK-3/PTFE cathode system exhibited a significantly superior RhB degradation rate (Fig. 8(b)). Remarkably, the degradation trends were consistent with those of H_2O_2 generation. Benefiting from the efficient *in situ* generation and activation of H_2O_2, the ZrO_2/CMK-3/PTFE cathode system displayed a robust ability to eliminate RhB in the flow-type cyclic degradation system. It is worth noting that by adjusting the pH, the produced iron sludge can be dissolved in the acidic electrolyte and then returned to the recycling system, which greatly enhances the operating stability of the system. This will increasingly inspire efforts toward the practical application

and scale-up of flow-type cyclic degradation systems for the engineering treatment of refractory wastewater.

In addition, the influence of the applied potential and solution pH on ZrO_2/CMK-3/PTFE EF degradation of organic pollutants was explored in a flow-type cyclic degradation system. The results show that as the applied potential negatively shifted from −0.3 to −0.8 V versus SHE, the RhB degradation rate increased from 82.9% to 96.2% (Fig. 9(a)), and the kinetic constant (k) of RhB degradation increased from −0.0577 to −0.1048 min^{-1} (Fig. 9(b)). Additionally, in the pH range studied, the RhB removal efficiency increased from 67.3% to 92.2%, and the k values varied from −0.0391 to −0.0833 min^{-1} (Figs. 9(c) and (d)). The improvement in the degradation efficiency might be attributed to the
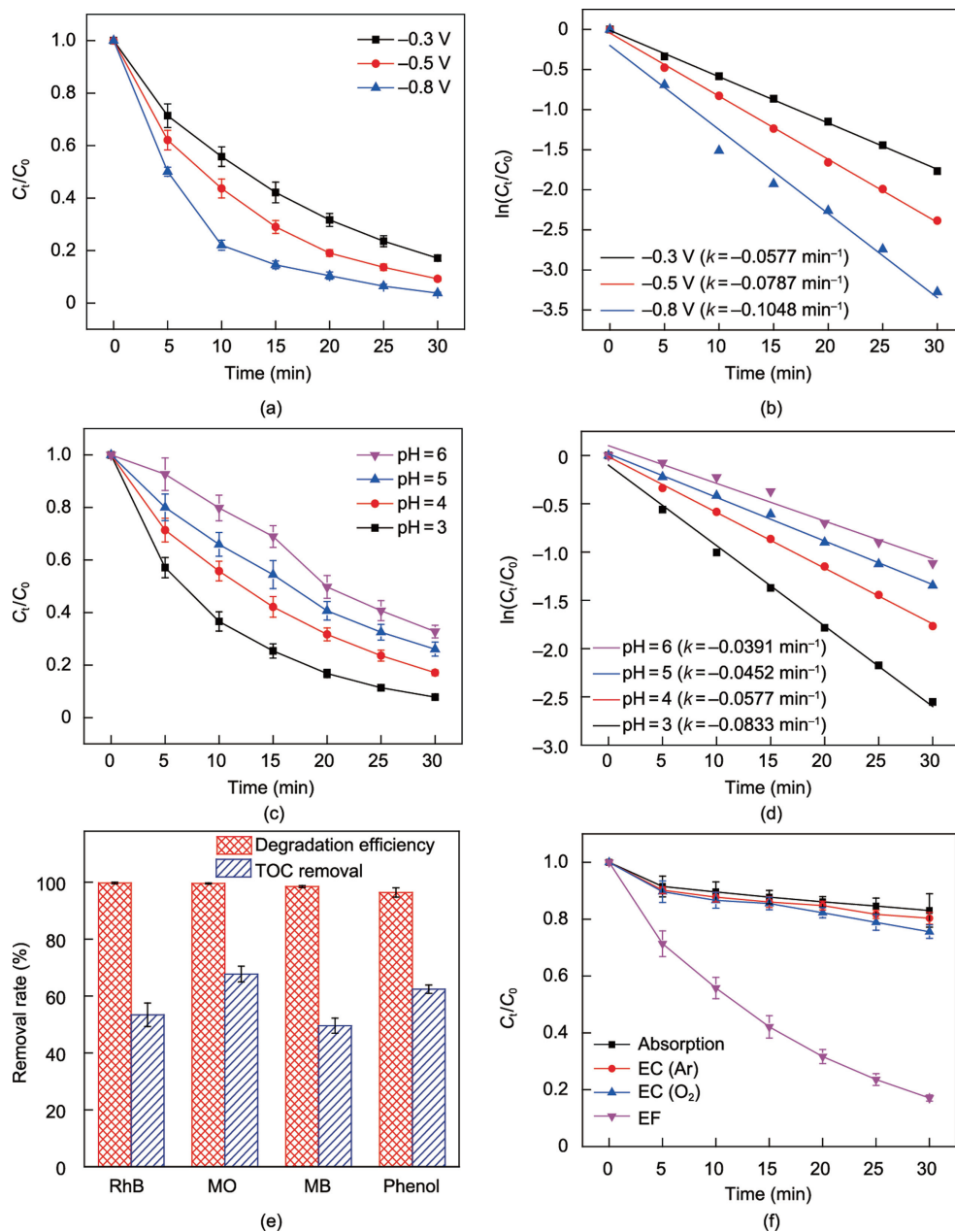

Fig. 9. (a) Effect of potential (pH = 4 and 1.0 $mmol·L^{-1}$ Fe^{2+}) on the degradation efficiency of RhB and (b) corresponding plots of $ln(C_t/C_0)$ vs time. Effect of (c) pH values (1.0 $mmol·L^{-1}$ Fe^{2+} and −0.3 V vs SHE) on the degradation efficiency of RhB and (d) corresponding plots of $ln(C_t/C_0)$ vs time. (e) The degradation efficiency and TOC removal rate of RhB, MO, MB, and phenol in the EF system (pH = 3, −0.8 V vs SHE and 1.0 $mmol·L^{-1}$ Fe^{2+}). (f) The degradation efficiency of RhB by EC (conducted under Ar or O_2) and EF (pH = 4, 1.0 $mmol·L^{-1}$ Fe^{2+}, and −0.3 V vs SHE).

increased H_2O_2 generation with the potential negative shift and the increased H^+ concentration, which could generate more ·OH to eliminate RhB. The degradation performance was further explored by degrading RhB, MO, MB, and phenol on the ZrO_2/CMK-3/PTFE EF system (pH 3 and −0.8 V versus SHE). As Fig. 9(e) illustrates, the removal efficiencies of RhB, MO, MB, and phenol were 99.8%, 99.6%, 98.5%, and 96.4% and TOC removal was 53.4%, 49.6%, 67.7%, and 62.4% within 120 min, respectively. A comparison with the literature on the degradation efficiency and TOC removal of pollutants is presented in Appendix A Table S2; the ZrO_2/CMK-3/PTFE EF system exhibited an efficient removal rate for the degradation and mineralization of refractory organic pollutants. Moreover, to further validate the performance of the system for pollutant degradation, RhB removal efficiencies by absorption, EC (under Ar or O_2 purge without Fe^{2+} added), and EF was compared at −0.3 V versus SHE and pH 4. As shown in Fig. 9(f), the RhB removal rates by absorption, EC (Ar), and EC (O_2) were all low, indicating that absorption and EC had little effect on RhB degradation. When the contaminant concentration was as low as 50 mg·L^{-1}, the ZrO_2/CMK-3/PTFE EF system achieved remarkable degradation efficiencies (Fig. S6 in Appendix A).

The reactive radicals generated in the EF reaction were identified by spin-trapping ESR spectroscopy using 5,5-dimethyl-1-pyrroline N-oxide (DMPO) as the trapping agent. As depicted in Fig. 10(a), the EF system displayed a 4-fold characteristic peak with a relative intensity of 1:2:2:1, which could be ascribed to the interaction between DMPO and ·OH [59]. After running for 5 min, the signal intensity of ·OH generated by the ZrO_2/CMK-3/PTFE EF system was significantly higher than those of the CMK-3 and CMK-3/PTFE systems. As the reaction progressed, the intensity of

the ·OH peak did not decrease significantly (Fig. 10(b)). These results are consistent with those for H_2O_2 production and pollutant degradation. No noticeable signal was observed in the absence of Fe^{2+} (Fig. 10(c)), demonstrating that ·OH was generated in the ZrO_2/CMK-3/PTFE EF system. Notably, quenching experiments of other possible reactive radicals (benzoquinone for ·O_2^-, L-histidine for $^1O_2$) showed that the degradation efficiency of RhB was not significantly inhibited by the quenchers (as displayed in Appendix A Fig. S7), which suggests that ·O_2^- and $^1O_2$ were not determining factors in the target contaminant degradation. The ·OH radical accounted for RhB degradation in the ZrO_2/CMK-3/PTFE EF system. To further verify the influence of ·OH on the EF degradation of RhB, tert-butyl alcohol (TBA) in a series of concentrations was applied to quench the ·OH produced during the degradation process. The results show that the RhB degradation efficiency decreased gradually with increasing TBA concentration (Fig. 10(d)), further indicating that ·OH was the principal active radical in the degradation of pollutants by EF. Consequently, all results illustrate that ZrO_2/CMK-3/PTFE has exceptional selectivity for both the production and activation of H_2O_2, thereby generating considerable ·OH for pollutant elimination, which is consistent with a previous study by Cao et al. [60].

4. Conclusions

Based on the fabrication of the novel ZrO_2/CMK-3/PTFE cathode, a systematic solution for efficient H_2O_2 generation and its EF application for refractory organic degradation was proposed. The hydrophilic/hydrophobic interface design of the ZrO_2/CMK-3/PTFE

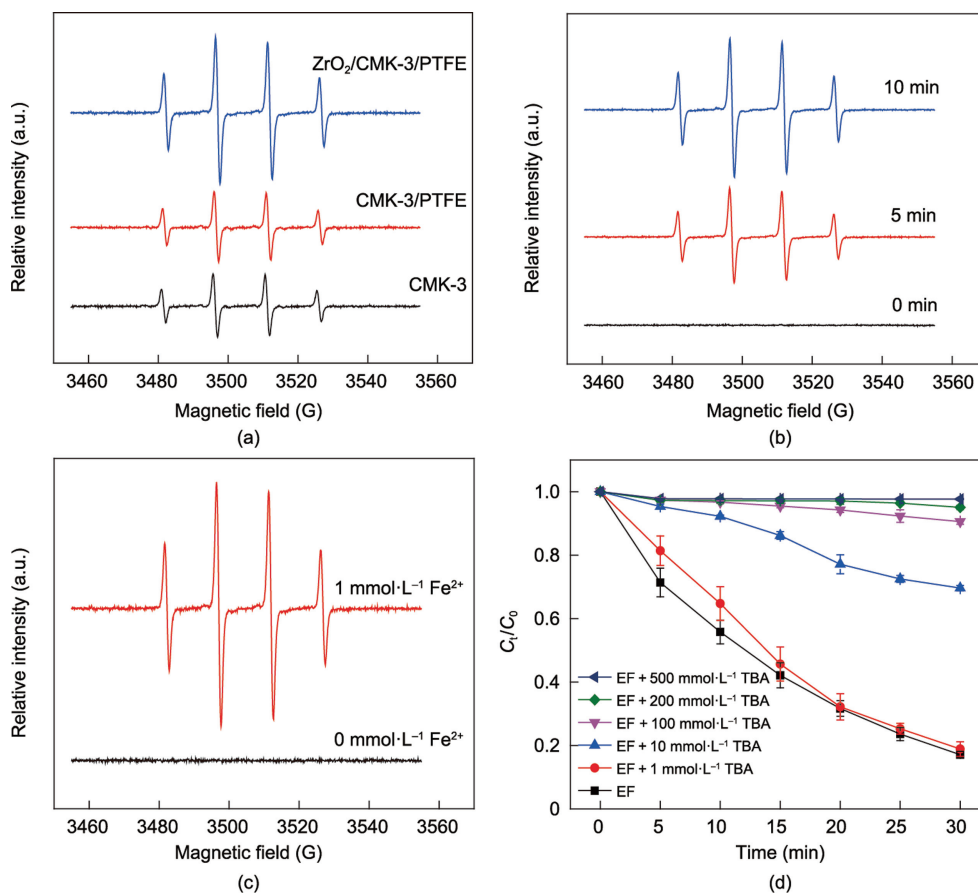**Fig. 10.** DMPO spin-trapping ESR spectra during EF process: (a) different cathode systems run for 5 min. (b) ZrO_2/CMK-3/PTFE cathode system run for 0, 5, and 10 min, respectively. (c) ZrO_2/CMK-3/PTFE cathode system run for 5 min with or without Fe^{2+} addition. (d) Effect of TBA concentration on EF degradation of RhB. Conditions: pH = 4, 1.0 mmol·L^{-1} Fe^{2+}, and −0.3 V versus SHE.

cathode solved the issues of O_2 mass transfer, cathodic catalyst selectivity, and electron transfer during O_2 reduction. The results showed exceptional EF performance for the degradation and mineralization of refractory organics. Our work is a step forward in enriching cathodes for efficient H_2O_2 production and will increasingly inspire efforts toward efficient cathode designs used for the engineering treatment of refractory wastewater.

Acknowledgments

Compliance with ethics guidelines

Lei Li, Jing Bai, Panyu Jiang, Yan Zhang, Tingsheng Zhou, Jiachen Wang, Changhui Zhou, Jinhua Li, and Baoxue Zhou declare that they have no conflict of interest or financial conflicts to disclose.

Appendix A. Supplementary data

Supplementary data to this article can be found online at https://doi.org/10.1016/j.eng.2023.02.005.

References

[1] Chen WQ, Li LY, Li L, Qiu WH, Tang L, Xu L, et al. MoS₂/ZIF-8 hybrid materials for environmental catalysis: solar-driven antibiotic-degradation engineering. Engineering 2019;5(4):755–67.
[2] Deletic A, Wang H. Water pollution control for sustainable development. Engineering 2019;5(5):839–40.
[3] Zha L, Bai J, Zhou C, Zhang Y, Li J, Wang P, et al. Treatment of hazardous organic amine wastewater and simultaneous electricity generation using photocatalytic fuel cell based on TiO₂/WO₃ photoanode and Cu nanowires cathode. Chemosphere 2022;289:133119.
[4] Brillas E, Sirés I, Oturan MA. Electro-Fenton process and related electrochemical technologies based on Fenton's reaction chemistry. Chem Rev 2009;109(12):6570–631.
[5] Su H, Christodoulatos C, Smolinski B, Arienti P, O'Connor G, Meng X. Advanced oxidation process for DNAN using UV/H₂O₂. Engineering 2019;5(5):849–54.
[6] Flox C, Ammar S, Arias C, Brillas E, Vargas-Zavala AV, Abdelhedi R. Electro-Fenton and photoelectro-Fenton degradation of indigo carmine in acidic aqueous medium. Appl Catal B 2006;67(1–2):93–104.
[7] Miao W, Wang Y, Liu Y, Qin H, Chu C, Mao S. Persulfate-induced three coordinate nitrogen (N₃C) vacancies in defective carbon nitride for enhanced photocatalytic H₂O₂ evolution. Engineering 2022;25(6):214–21.
[8] Campos-Martin JM, Blanco-Brieva G, Fierro JL. Hydrogen peroxide synthesis: an outlook beyond the anthraquinone process. Angew Chem Int Ed Engl 2006;45(42):6962–84.
[9] Gogoi S, Karak N. Solar-driven hydrogen peroxide production using polymer-supported carbon dots as heterogeneous catalyst. Nano-Micro Lett 2017;9(4):40.
[10] Piao H, Choi G, Jin X, Hwang SJ, Song YJ, Cho SP, et al. Monolayer graphitic carbon nitride as metal-free catalyst with enhanced performance in photo- and electro-catalysis. Nano-Micro Lett 2022;14(1):55.
[11] Brillas E. Progress of homogeneous and heterogeneous electro-Fenton treatments of antibiotics in synthetic and real wastewaters. A critical review on the period 2017–2021. Sci Total Environ 2022;819:153102.
[12] Barhoumi N, Oturan N, Olvera-Vargas H, Brillas E, Gadri A, Ammar S, et al. Pyrite as a sustainable catalyst in electro-Fenton process for improving oxidation of sulfamethazine. Kinetics, mechanism and toxicity assessment. Water Res 2016;94:52–61.
[13] Chen L, Medlin JW, Grönbeck H. On the reaction mechanism of direct H₂O₂ formation over Pd catalysts. ACS Catal 2021;11(5):2735–45.
[14] Chang Q, Zhang P, Mostaghimi AHB, Zhao X, Denny SR, Lee JH, et al. Promoting H₂O₂ production via 2-electron oxygen reduction by coordinating partially oxidized Pd with defect carbon. Nat Commun 2020;11(1):2178.
[15] Sun Z, Wang Y, Zhang L, Wu H, Jin Y, Li Y, et al. Simultaneously realizing rapid electron transfer and mass transport in Jellyfish-like Mott–Schottky

[16] Zhou H, Zhang H, He Y, Huang B, Zhou C, Yao G, et al. Critical review of reductant-enhanced peroxide activation processes: trade-off between accelerated Fe³⁺/Fe²⁺ cycle and quenching reactions. Appl Catal B 2021;286:119900.
[17] Xing R, Zhou T, Zhou Y, Ma R, Liu Q, Luo J, et al. Creation of triple hierarchical micro–meso–macroporous N-doped carbon shells with hollow cores toward the electrocatalytic oxygen reduction reaction. Nano-Micro Lett 2018;10(1):3.
[18] Gu D, Zhou Y, Ma R, Wang F, Liu Q, Wang J. Facile synthesis of N-doped graphene-like carbon nanoflakes as efficient and stable electrocatalysts for the oxygen reduction reaction. Nano-Micro Lett 2018;10(2):29.
[19] Xia Y, Zhao X, Xia C, Wu ZY, Zhu P, Kim JYT, et al. Highly active and selective oxygen reduction to H₂O₂ on boron-doped carbon for high production rates. Nat Commun 2021;12(1):4225.
[20] Li L, Bai J, Chen S, Zhang Y, Li J, Zhou T, et al. Enhanced O₂⁻· and HO· via *in situ* generating H₂O₂ at activated graphite felt cathode for efficient photocatalytic fuel cell. Chem Eng J 2020;399:125839.
[21] Zhang Z, Meng H, Wang Y, Shi L, Wang X, Chai S. Fabrication of graphene@graphite-based gas diffusion electrode for improving H₂O₂ generation in electro-Fenton process. Electrochim Acta 2018;260:112–20.
[22] Han GF, Li F, Zou W, Karamad M, Jeon JP, Kim SW, et al. Building and identifying highly active oxygenated groups in carbon materials for oxygen reduction to H₂O₂. Nat Commun 2020;11(1):2209.
[23] Lan H, He W, Wang A, Liu R, Liu H, Qu J, et al. An activated carbon fiber cathode for the degradation of glyphosate in aqueous solutions by the electro-Fenton mode: optimal operational conditions and the deposition of iron on cathode on electrode reusability. Water Res 2016;105:575–82.
[24] Zhang Y, Liu L, Van der Bruggen B, Yang F. Nanocarbon based composite electrodes and their application in microbial fuel cells. J Mater Chem A Mater Energy Sustain 2017;5(25):12673–98.
[25] Liu Y, Quan X, Fan X, Wang H, Chen S. High-yield electrosynthesis of hydrogen peroxide from oxygen reduction by hierarchically porous carbon. Angew Chem Int Ed Engl 2015;54(23):6837–41.
[26] Luo P, Pang Z, Qin Z, Wei T, Li S, Hu Y, et al. Strategies for improving Co/Ni-based bimetal-organic framework to water splitting. Int J Hydrogen Energy 2020;45(53):28240–51.
[27] Sun Y, Sinev I, Ju W, Bergmann A, Dresp S, Kühl S, et al. Efficient electrochemical hydrogen peroxide production from molecular oxygen on nitrogen-doped mesoporous carbon catalysts. ACS Catal 2018;8(4):2844–56.
[28] Zhang Q, Zhou M, Ren G, Li Y, Li Y, Du X. Highly efficient electrosynthesis of hydrogen peroxide on a superhydrophobic three-phase interface by natural air diffusion. Nat Commun 2020;11(1):1731.
[29] Moreira J, Lima VB, Goulart LA, Lanza MRV. Electrosynthesis of hydrogen peroxide using modified gas diffusion electrodes (MGDE) for environmental applications: quinones and azo compounds employed as redox modifiers. Appl Catal B 2019;248:95–107.
[30] Lu X, Zhou M, Li Y, Su P, Cai J, Pan Y. Improving the yield of hydrogen peroxide on gas diffusion electrode modified with tert-butyl-anthraquinone on different carbon support. Electrochim Acta 2019;320:134552.
[31] Gu Z, Zhou J, An X, Chen Q, Hu C, Liu H, et al. A dual-biomimetic photocatalytic fuel cell for efficient electricity generation from degradation of refractory organic pollutants. Appl Catal B 2021;298:120501.
[32] Xu A, He B, Yu H, Han W, Li J, Shen J, et al. A facile solution to mature cathode modified by hydrophobic dimethyl silicon oil (DMS) layer for electro-Fenton processes: water proof and enhanced oxygen transport. Electrochim Acta 2019;308:158–66.
[33] Sheng Y, Zhao Y, Wang X, Wang R, Tang T. Electrogeneration of H₂O₂ on a composite acetylene black–PTFE cathode consisting of a sheet active core and a dampproof coating. Electrochim Acta 2014;133:414–21.
[34] Carneiro JF, Paulo MJ, Siaj M, Tavares AC, Lanza MRV. Nb₂O₅ nanoparticles supported on reduced graphene oxide sheets as electrocatalyst for the H₂O₂ electrogeneration. J Catal 2015;332:51–61.
[35] Paz EC, Aveiro LR, Pinheiro VS, Souza FM, Lima VB, Silva FL, et al. Evaluation of H₂O₂ electrogeneration and decolorization of Orange II azo dye using tungsten oxide nanoparticle-modified carbon. Appl Catal B 2018;232:436–45.
[36] Barros WRP, Wei Q, Zhang G, Sun S, Lanza MRV, Tavares AC. Oxygen reduction to hydrogen peroxide on Fe₃O₄ nanoparticles supported on Printex carbon and graphene. Electrochim Acta 2015;162:263–70.
[37] Aveiro LR, da Silva AGM, Antonin VS, Candido EG, Parreira LS, Geonmonond RS, et al. Carbon-supported MnO₂ nanoflowers: introducing oxygen vacancies for optimized volcano-type electrocatalytic activities towards H₂O₂ generation. Electrochim Acta 2018;268:101–10.
[38] Zheng D, Cao XN, Wang X. Precise formation of a hollow carbon nitride structure with a Janus surface to promote water splitting by photoredox catalysis. Angew Chem Int Ed Engl 2016;55(38):11512–6.
[39] Carneiro JF, Trevelin LC, Lima AS, Meloni GN, Bertotti M, Hammer P, et al. Synthesis and characterization of ZrO₂/C as electrocatalyst for oxygen reduction to H₂O₂. Electrocatalysis 2017;8(3):189–95.
[40] Carneiro JF, Paulo MJ, Siaj M, Tavares AC, Lanza MRV. Zirconia on reduced graphene oxide sheets: synergistic catalyst with high selectivity for H₂O₂ electrogeneration. Chem Electro Chem 2017;4(3):508–13.
[41] Kronka MS, Cordeiro-Junior PJM, Mira L, dos Santos AJ, Fortunato GV, Lanza MRV. Sustainable microwave-assisted hydrothermal synthesis of carbon-supported ZrO₂ nanoparticles for H₂O₂ electrogeneration. Mater Chem Phys 2021;267:124575.

[42] Antonin VS, Assumpção MHMT, Silva JCM, Parreira LS, Lanza MRV, Santos MC. Synthesis and characterization of nanostructured electrocatalysts based on nickel and tin for hydrogen peroxide electrogeneration. Electrochim Acta 2013;109:245–51.

[43] Scialdone O, Galia A, Gattuso C, Sabatino S, Schiavo B. Effect of air pressure on the electro-generation of H_2O_2 and the abatement of organic pollutants in water by electro-Fenton process. Electrochim Acta 2015;182:775–80.

[44] An J, Li N, Zhao Q, Qiao Y, Wang S, Liao C, et al. Highly efficient electro-generation of H_2O_2 by adjusting liquid–gas–solid three phase interfaces of porous carbonaceous cathode during oxygen reduction reaction. Water Res 2019;164:114933.

[45] Zhou T, Li L, Li J, Wang J, Bai J, Xia L, et al. Electrochemically reduced TiO_2 photoanode coupled with oxygen vacancy-rich carbon quantum dots for synergistically improving photoelectrochemical performance. Chem Eng J 2021;425:131770.

[46] Wang J, Zhou T, Zhang Y, Li L, Zhou C, Bai J, et al. Type-II heterojunction $CdIn_2S_4$/ $BiVO_4$ coupling with CQDs to improve PEC water splitting performance synergistically. ACS Appl Mater Interfaces 2022;14(40):45392–402.

[47] Moraes A, Assumpção MHMT, Simões FC, Antonin VS, Lanza MRV, Hammer P, et al. Surface and catalytical effects on treated carbon materials for hydrogen peroxide electrogeneration. Electrocatalysis 2016;7(1):60–9.

[48] Yu F, Zhou M, Yu X. Cost-effective electro-Fenton using modified graphite felt that dramatically enhanced on H_2O_2 electro-generation without external aeration. Electrochim Acta 2015;163:182–9.

[49] Mei X, Bai J, Chen S, Zhou M, Jiang P, Zhou C, et al. Efficient SO_2 removal and highly synergistic H_2O_2 production based on a novel dual-function photoelectrocatalytic system. Environ Sci Technol 2020;54(18):11515–25.

[50] Wang H, Pan M, Tan H. Application of PTFE and Nafion in the catalyst layer for PEMFC. Cell 2007;02:158–60.

[51] Carneiro JF, Silva FL, Martins AS, Dias RMP, Titato GM, Santos-Neto ÁJ, et al. Simultaneous degradation of hexazinone and diuron using ZrO_2-nanostructured gas diffusion electrode. Chem Eng J 2018;351:650–9.

[52] Chen S, Luo T, Chen K, Lin Y, Fu J, Liu K, et al. Chemical identification of catalytically active sites on oxygen-doped carbon nanosheet to decipher the high activity for electro-synthesis hydrogen peroxide. Angew Chem Int Ed Engl 2021;60(30):16607–14.

[53] Yang H, Zhou M, Yang W, Ren G, Ma L. Rolling-made gas diffusion electrode with carbon nanotube for electro-Fenton degradation of acetylsalicylic acid. Chemosphere 2018;206:439–46.

[54] Shi X, Zhang Y, Siahrostami S, Zheng X. Light-driven $BiVO_4$–C fuel cell with simultaneous production of H_2O_2. Adv Energy Mater 2018;8(23): 1801158.

[55] Zhao Q, Wang Y, Lai WH, Xiao F, Lyu Y, Liao C, et al. Approaching a high-rate and sustainable production of hydrogen peroxide: oxygen reduction on Co–N– C single-atom electrocatalysts in simulated seawater. Energy Environ Sci 2021;14(10):5444–56.

[56] Zhang G, Wang S, Zhao S, Fu L, Chen G, Yang F. Oxidative degradation of azo dye by hydrogen peroxide electrogenerated *in situ* on anthraquinonemonosulphonate/ polypyrrole composite cathode with heterogeneous $CuO/\gamma-Al_2O_3$ catalyst. Appl Catal B 2011;106(3–4):370–8.

[57] Du X, Oturan MA, Zhou M, Belkessa N, Su P, Cai J, et al. Nanostructured electrodes for electrocatalytic advanced oxidation processes: from materials preparation to mechanisms understanding and wastewater treatment applications. Appl Catal B 2021;296:120332.

[58] Yu A, Ma G, Zhu L, Zhang R, Li Y, Yang S, et al. Conversion of CO_2 to defective porous carbons in one electro-redox cycle for boosting electrocatalytic H_2O_2 production. Appl Catal B 2022;307:121161.

[59] Jourshabani M, Asrami MR, Lee BK. An efficient and unique route for the fabrication of highly condensed oxygen-doped carbon nitride for the photodegradation of synchronous pollutants and H_2O_2 production under ambient conditions. Appl Catal B 2022;302:120839.

[60] Cao P, Quan X, Zhao K, Chen S, Yu H, Niu J. Selective electrochemical H_2O_2 generation and activation on a bifunctional catalyst for heterogeneous electro-Fenton catalysis. J Hazard Mater 2020;382:121102.